Metastable Clusters and Competitive Solvation Tune Ion Pairing at Liquid Interfaces

Pan Sun[1*], Robert L. Sacci[1], Uvinduni I. Premadasa[1], Jan–Michael Y. Carrillo[2*], Santanu Roy[1*], Benjamin Doughty[1*]

1. Chemical Sciences Division, Oak Ridge National Laboratory, Oak Ridge, Tennessee 37830, United States of America.
2. Center for Nanophase Materials Science, Oak Ridge National Laboratory, Oak Ridge, Tennessee 37830, United States of America.

Metastable Clusters and Competitive Solvation Tune Ion Pairing at Liquid Interfaces

Pan Sun[1*], Robert L. Sacci[1], Uvinduni I. Premadasa[1], Jan–Michael Y. Carrillo[2*], Santanu Roy[1*], Benjamin Doughty[1*]

1. Chemical Sciences Division, Oak Ridge National Laboratory, Oak Ridge, Tennessee 37830, United States of America.
2. Center for Nanophase Materials Science, Oak Ridge National Laboratory, Oak Ridge, Tennessee 37830, United States of America.
KEYWORDS: Metastable Clusters, Solvation, Hydrogen bonding, Heterogeneity, Interfaces

ABSTRACT: The balance of hydrophobic and hydrophilic interactions underlies emergent phenomena in complex multicomponent chemical systems. Here, we show that a supposedly 'non–interacting' nonpolar phase can be used to competitively solvate amphiphilic molecules at an oil/aqueous interface. This solvation, as probed by surface specific nonlinear spectroscopy and simulations, results in a molecularly thin corrugated phase boundary featuring metastable assemblies that alter the hydrogen bonding networks of water and the apparent 'hard/soft' descriptors used to describe ionic interactions. We show that competitive solvation enhances amphiphile mobility, opening up otherwise energetically inaccessible complexes that transiently interact with aqueous phase ions. These transient species impact ensemble binding affinities and may represent the molecular agents responsible for aspects of ionic transport and function. The results of this work highlight how seemingly unrelated nonpolar interactions feedback onto aqueous phase chemical phenomena, providing a pathway to tune phase separation and self-assembly to access new reaction pathways using interfaces for a range of chemical and biological systems.

INTRODUCTION

Complex, multicomponent chemical systems often leverage a delicate balance between hydrophobicity, hydrophilicity (*i.e.,* phase segregation) and ionic interactions to drive emergent functionality.[1-4] For instance, proteins folding relies on the way in which water, ions, and hydrophobic residues balance their individual needs in the context of the greater overall thermodynamic landscape.[5-6] Similarly, the ways in which molecules self–assemble to recognize chemical species in large scale chemical separations[7-8] or in brain–mimicking neuromorphic computing devices rely on analogous delicate balancing acts.[9] The asymmetric local chemical environment found at interfaces provides an ability to re-tune these interactions via differential ordering, assembly and stratification of molecular constituents.[10-13] While potentially powerful, a mechanistic understanding describing the balance of these interactions has remained elusive due in part to challenges in measuring interfacial phenomena, transient structures, and competitive interactions taking place between interfacial constituents that are often chemically and structurally similar.

In this regard, solvation on both sides of an interface (*e.g.*, in the hydrophilic and hydrophobic phases) as sketched in Figure 1 is known to play a prominent role in defining macroscopic surface properties and chemical function at buried liquid interfaces, yet remains remarkably poorly understood.[14-15] At these interfaces, assembly is typically framed from the perspective of the aqueous phase species dominating the energetic landscape, whereas the neighboring nonpolar phase is typically taken as a 'non–interacting' phase that is purely a spectator.[16-18] However, the balance of hydrophobic and ionic interactions intimately depends on the composition of *both* phases – adjustments to solvation on either side of the interface can lead to dramatic changes in chemical function[19-21] or macroscopic phase transitions[22-23] that underly nanoscale assembly,[24-26] ionic transport,[27-28] and molecular memory.[29] While model air/aqueous interfaces provide insight into piecewise interactions, inclusion of competitive species and different phase compositions can give rise to functional assemblies

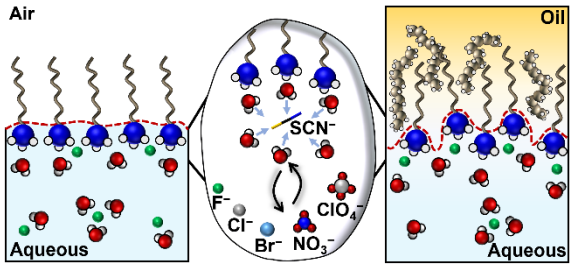

Figure 1: The local environments found at interfaces influence H-bonding and ionic interactions that are balanced by hydrophobic and phase dependent interactions. Understanding how these competing interactions result in emergent functionality in realistic, multicomponent, systems can bring about ways to control interfaces for selective and energy efficient next generation chemistry, processes, and devices. We probe these interfaces using SFG vibrational spectroscopy (b) to chemically map interfaces covered in octadecyl amine (ODA, c)

whose chemical properties are entirely inaccessible to these simpler model systems. This knowledge gap in how hydrophobic and ionic interactions differ at interfaces and how multicomponent mixtures compete limits our ability to design interfacial environments in basic or applied contexts.

Here, we leverage the competitive adsorption of ions to realistic air/aqueous and oil/aqueous interfaces to provide mechanistic insight into solvation on both sides of an interface. Using surface-specific nonlinear spectroscopic measurements and modeling and free-energy landscapes explored in molecular dynamics simulations, we show how specific ion effects are tuned based on emergent H–bonding networks that differ based on the nature of the 'non–interacting' nonpolar phase. These H–bonding networks modulate how the charged amphiphilic headgroups 'appear' from the perspective the ions in an aqueous phase and impact the mechanisms of ion exchange and binding. We find that the adsorption affinities of surface *inactive* ions vary by more than a kJ/mol depending on the nature of the nonpolar phase and the associated free energy surface on which they traverse. This effect is linked to apparent differences in H–bonding strengths and a heterogeneous arrangement of interfacial surfactants and metastable ion-surfactant clusters that emerge through tail solvation with the oil phase. Unique spatially isolated ion pairs and solvent-exposed headgroups are identified at oil/aqueous interfaces, suggesting key pathways by which species are transported through interfaces with implications for drug delivery, critical material separations, and soft matter electronics. The tug–of–war between competing hydrophilic and hydrophobic interactions, each pulling on the molecules from the neighboring phases, results in a dynamic physical picture where competitive solvation can be used to construct stratified solvation environments to facilitate selective chemical transformations.

RESULTS AND DISCUSSIONS

To understand the competition between solvation, ionic interactions and H–bonding, we choose to probe air/aqueous and *n*-decane/aqueous interfaces as exemplar systems that are often assumed to be chemically and functionally identical. These interfaces are coated with octadecyl amine (ODA), a positively charged amphiphile, to electrostatically attract anions to the surface and stabilize the decane/aqueous interface, as sketched in Figure 2a. Based on surface tension measurements (Figure S1), the average area each ODA occupies for both model

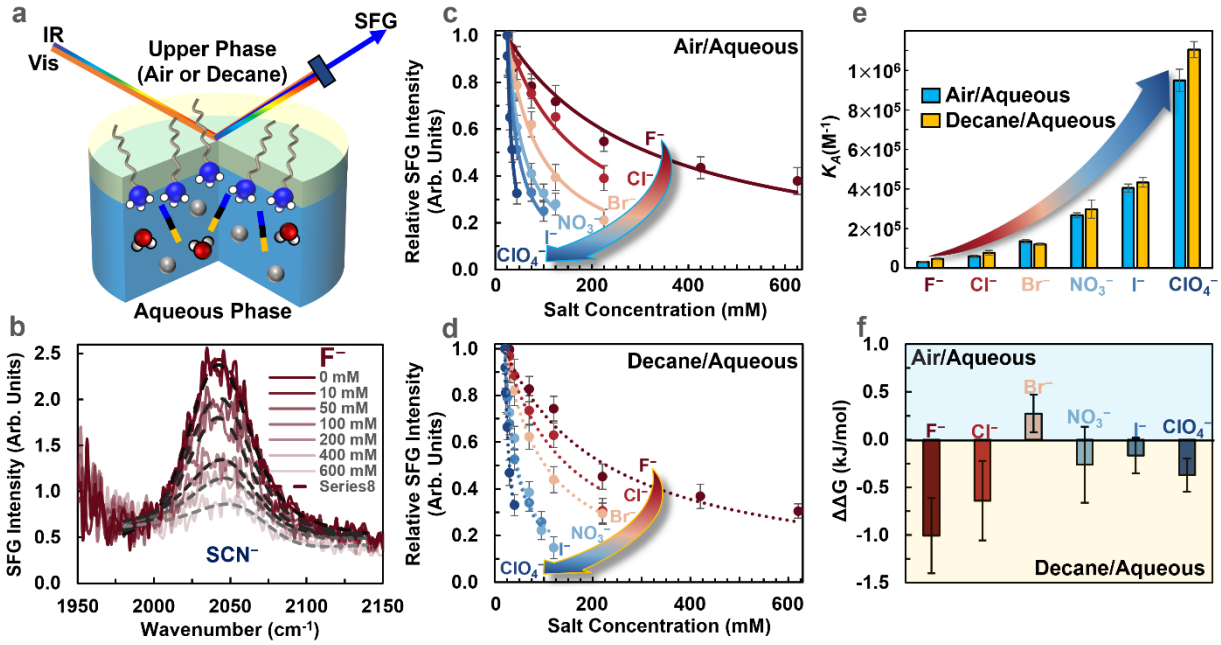

Figure 2: a) Schematic of the *n*-decane/aqueous interfaces probed using SFG, where infrared (IR) and near infrared (NIR) pulses interact with interfacial species to generate signals specific to the surface. The reduction of signal from SCN^-, as measured by SFG, in competition with F^- is plotted in b). Displacement isotherms measured at c) air/aqueous and d) oil/aqueous interfaces follow expected trends in ion hydration. Adsorption equilibrium constants (K_A) and calculated $\Delta\Delta G_{ads}$ for the different ions at the oil/aqueous vs. air/aqueous interfaces are plotted in e) and f), respectively, which show a notable difference in binding free energies.

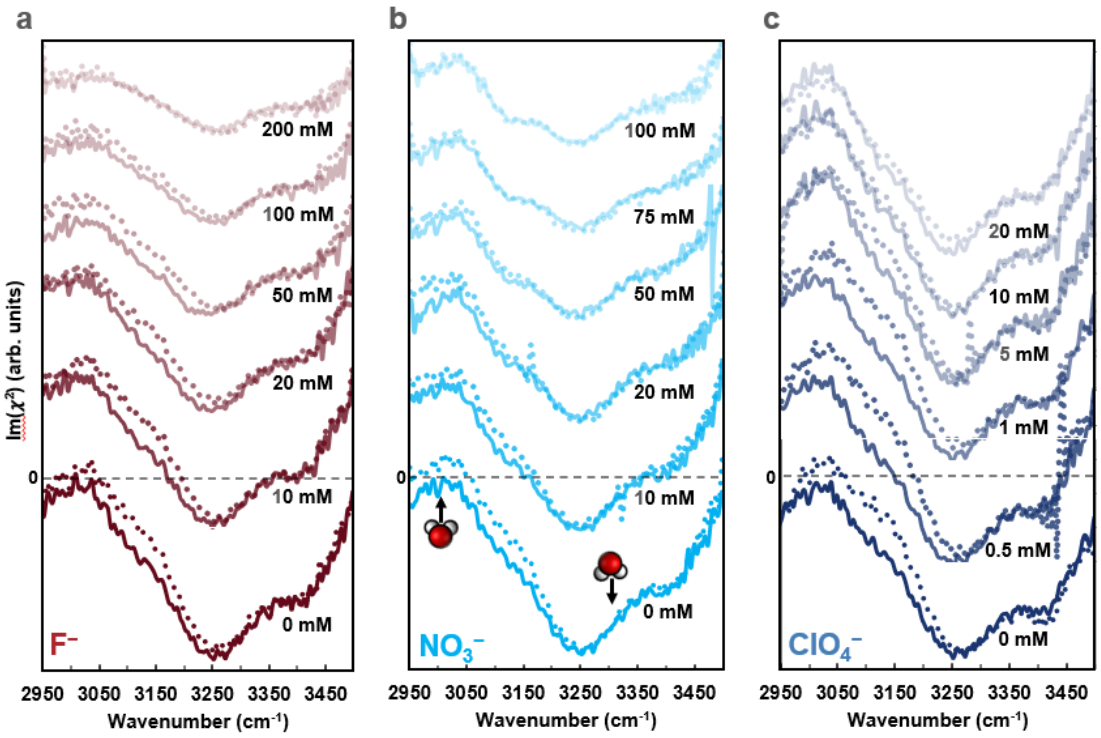

Figure 3: Variation of imaginary part of the SFG response in the OH stretching region in the presence of F^-, NO_3^- and ClO_4^- for the air/aqueous interface (dotted lines) and oil/aqueous interfaces (solid line). The difference in low frequency vibrations suggests that H-bonding is stronger at oil/aqueous interfaces vs. air/aqueous interfaces.

interfaces probed in this work is ~21 Å^2/molecule, allowing for a 1:1 comparison between samples. To quantify differential ion adsorption between the two interfaces, we first measure the adsorption equilibria of SCN^- on the ODA decorated interfaces using sum frequency generation (SFG) vibrational spectroscopy, discussed in the Methods section. SCN^- is probed because it is a surface–active anion with a characteristic vibration at 2050 cm^{-1} that can be measured as a function of bulk concentration to yield SFG adsorption and displacement isotherms. Adsorption isotherms probing SCN^- at the air/aqueous vs. oil/aqueous interfaces (Figure S2) retrieve similar equilibrium adsorption constants and number densities (values given in Table S2), indicating that the systems behave similarly. However, SFG spectra probing mixtures of SCN^- competing for adsorption sites with anions across the Hofmeister series, plotted in Figure 2b, show a marked decrease in the SCN^- response for all studied anions (Figure S3–S6) that differ based on the nonpolar phase. The decrease in SCN^- signals report on reduced interfacial populations from competitive adsorption of other anions to a limited number of surface sites, as confirmed by separate orientational measurements (Figure S7). To quantify the adsorption of these competitive ions, we plot the reduction of the SCN^- response in Figure 2c and 2d for air/aqueous and decane/aqueous interfaces, respectively, as displacement isotherms. From these measurements and analysis detailed in the SI, adsorption equilibrium constants, K_A, for competitive ions at both interfaces are summarized in Figure 2e.

For both interfaces we find that ion adsorption follows $F^- < Cl^- < Br^- < NO_3^- < I^- < ClO_4^- \approx SCN^-$, which is consistent with Hofmeister trends in anion hydration.[30-31] Free energies of adsorption, ΔG_{ads}, at 298 K are calculated using measured values of K_A. To highlight the differences in interfacial affinity we plot changes in ΔG_{ads} , $\Delta\Delta G_{ads} = \Delta G_{decane/aqueous} - \Delta G_{air/aqueous}$, in Figure 2f, which shows hydrophilic ions, like F^- and Cl^-, prefer decane/aqueous interfaces over air/aqueous interfaces. We note that the Law of Matching Water Affinities, or Collin's rule,[32-33] suggests that hard anions prefer to form contact ion pairs with hard cations based on compatible enthalpies of hydration and size. In this context, the stronger binding of F^- to ODA at decane/aqueous interfaces might suggest that the $-NH_3^+$ headgroup 'appears' more strongly solvated (*e.g.*, a harder cation) as compared to the same headgroup at the air/aqueous interface. Correspondingly so, we hypothesize that the H–bonding network defined by the $-NH_3^+$ headgroups are tuned by interactions with the neighboring nonpolar phase.

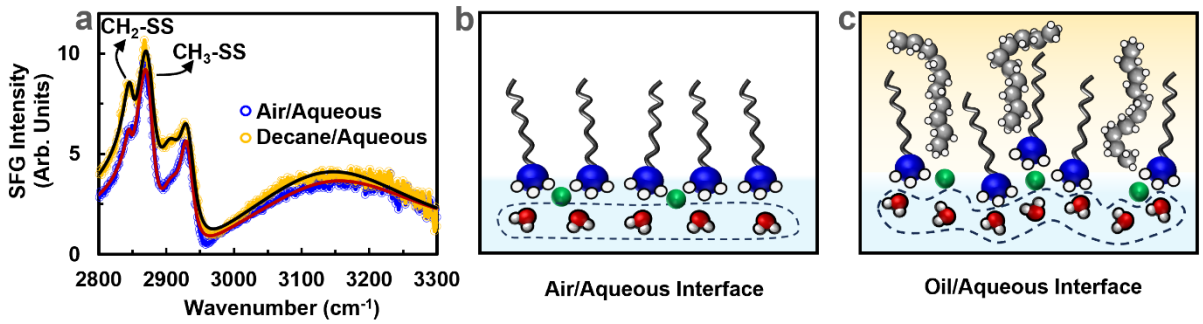

Figure 4: These differences in H-bonding strength map to ion adsorption, as described in the text. SFG spectra in the CH region (a), show that from the ratio of CH_2/CH_3 signals, that the oil/aqueous interface is more disordered and, on the molecular scale, rougher than the air/aqueous interface. These interfaces are sketched in b) and c) for air and decane nonpolar phases, respectively.

To test this hypothesis and probe H–bonding under the same conditions, we measured interfacial OH stretching vibrations of water using SFG. The imaginary parts of the effective second order susceptibility, $\mathrm{Im}(\chi^{(2)})$, are plotted in Figure 3a–3c that describes the absorbative part of the nonlinear optical response. The sign of $\mathrm{Im}(\chi^{(2)})$ informs on the orientation of the associated transition dipole moment (up vs. down)[34-35] as shown in Figure 3b. These spectra are extracted from intensity measurements using the maximum entropy method[36] after applying spectral corrections based on separately measured Fresnel factors.[37] A step–by–step procedure detailing the processing is provided in the SI. Three ions (F^-, NO_3^- and ClO_4^-) are considered here to inform on trends across the Hofmeister series. We note that the static electric field setup by the positively charged $-NH_3^+$ headgroups polarizes bulk water via the so called $\chi^{(3)}$–effect.[38-40] As the bulk ionic strength increases, the SFG response from field aligned water decreases due to charge screening and ion pairing – this is observed in Figure 3a–3c as a decrease in the magnitude of the negative signed SFG response. We emphasize that in all cases, 10 mM NaSCN is present in the system, so the most dramatic effects from the $\chi^{(3)}$–effect, found at low total ionic strengths, are minimized.[14, 38, 41] It should be noted that there are still strong contributions from field aligned water that change as a function of ionic strength.

We find that the OH responses and line shapes vary across both ion and the concentration series and report on specific ion effects, ionic layering, and associated H–bonding.[42] At low competitive anion concentrations, the OH spectral response from air/aqueous interfaces is notably different at decane/aqueous interfaces on the low frequency side of the spectrum. These low frequency vibrations report on strongly H–bonded water with contributions from –NH stretching modes of the ODA headgroup.[30] As such, differences in this region indicate that 1) water is organized at the two interfaces in fundamentally different ways, 2) that the $-NH_3^+$ headgroups present themselves differently to the aqueous phase depending on the nature of neighboring nonpolar phase, and the 3) H–bonding of water and $-NH_3^+$ groups at decane/aqueous interfaces appears stronger than at air/aqueous interfaces.[39, 42] We should emphasize here that comparison of different ionic solutions at different ionic strengths requires removing contributions from field aligned water, which is beyond the scope of the current work.[38, 43] As the concentration of competitive ions reaches saturation, the spectra from the two interfaces become indistinguishable, but retain spectroscopic differences depending on the anions and their effect on the local H–bonding network at saturation. To characterize the amphiphiles and packing at the surfaces CH stretching spectra plotted in Figure 4a. The ratio of $-CH_2$ to $-CH_3$ signals (bands at ~2850 cm^{-1} and ~2875 cm^{-1}, respectively) reports on tail packing and the presence of gauche conformers at the interface; the smaller $-CH_2$ to $-CH_3$ ratio indicates that the tails are better packed at air/aqueous interfaces.[34] From this analysis, we find that ODA tails are more poorly ordered and have a larger conformational space to sample at decane/aqueous interfaces, suggesting that interfaces are roughened on the molecular scale with some species extending deeper into one phase or another (verified *vida infra*). This physical picture, sketched in Figure 4b) and 4c), agrees with surface tension measurements (Figure S1) that point to a molecularly roughened decane/aqueous interface. Here, we make the connection that the way in which decane solvates the ODA tails feeds-back onto the surface to enable what appears as stronger H–bonding in the aqueous phase, as evidenced by the spectra in Figure 3a–c. Given that the oil/aqueous interface is more structurally heterogeneous, it would stand to reason that ODA is being tugged in two directions – between the two phases – as governed by the instantaneous

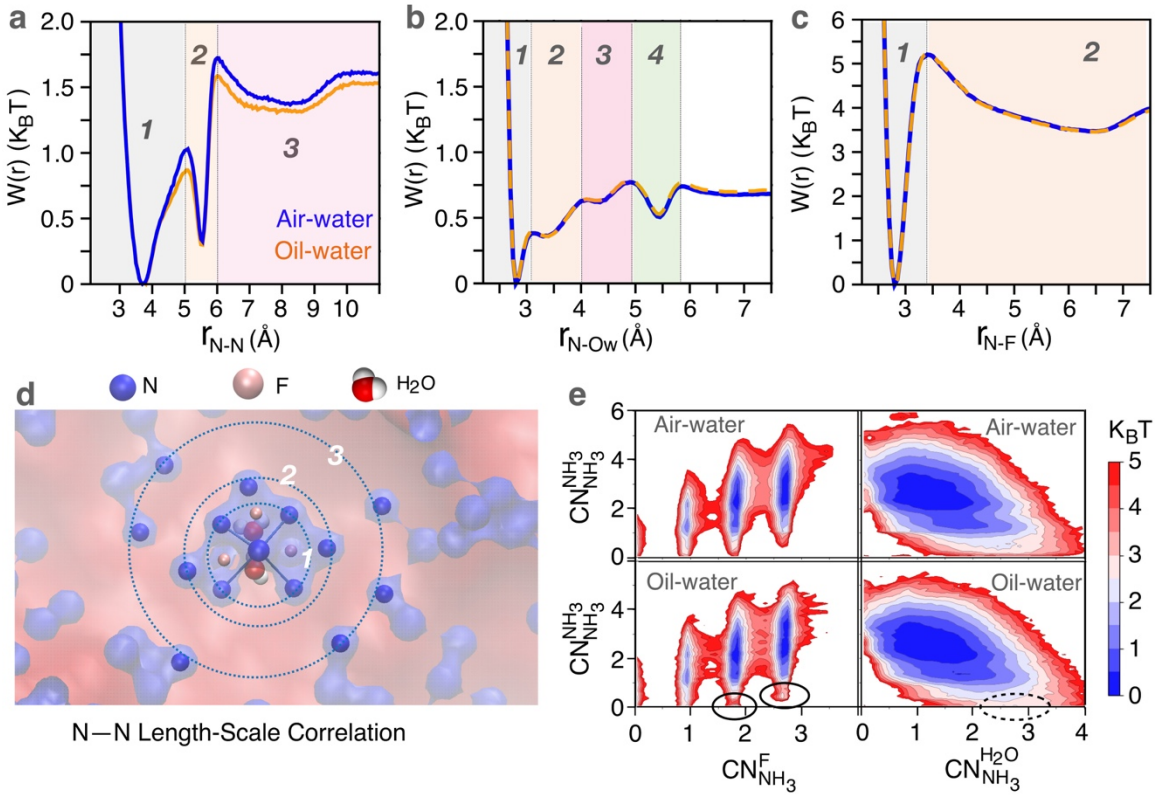

Figure 5. From MD simulations of the air-water and oil-water systems with a high F^- concentration, the free energy profiles (W(r)) for a) N-N separation distances showing three metastable coordination spheres describing microheterogeneity at decane/aqueous and air/aqueous interfaces. The N-water oxygen (O_w) separation b) distances show four metastable coordination spheres, whereas NH_3^+–F^- profiles shown in c) are significantly stronger than N-N and N-O_w interactions (a and b). The microheterogeneity is illustrated in d) with representative water and F^- ions sketched within respective shells indicated in a); regions 1 and 2 represent the short-range correlations while region 3 describes intermediate-range correlations with nearest neighbor clusters. Fictitious bonds are to illustrate the nearest neighbors. 2D free energy surfaces e) highlight the correlation between the clustering, via N-N coordination number with F^- and water coordination numbers. Isolated ODA-F^- coordination complexes (highlighted by solid circles) or isolated hydrated ligand (dashed-circle) species energetically accessible only at the decane/aqueous interface.

solvent environment and ionic localization. This leads to some head groups being more exposed to water and others buried deeper into the nonpolar phase. This apparent corrugation across the interface evolves as competitive ion concentrations increase, such that the pull from the aqueous phase eventually wins out over comparatively weaker hydrophobic interactions. As such, this interfacial heterogeneity results in different local H-bonding networks at a given interface. Based on measurements, these microheterogeneities are suppressed at air/aqueous interfaces and enhanced at decane/aqueous interfaces, in agreement with conclusions drawn from emulsions possessing large interfacial curvature.[42]

To support this notion of interfacial corrugation, we use atomistic MD simulations to explore reaction coordinates and associated free energy landscapes for the interfacial solvation and ion coordination processes (details are provided in the SI). Briefly, we perform 10 independent replicas over 10 ns windows (100 ns total) at a high ion concentration (~1.9 M) to ensure proper sampling of exchange dynamics and specific ion effects. We note here that the concentrations studied in experiments, for instance, those with F^-, are ~3x lower than that used in simulation. To confirm that comparisons can be made between the results, additional measurements were made in the CH stretching region at different concentrations of competitive ions (data given in Figure S14), that show the decane/aqueous interfaces are always more disordered and that competitive ions effectively compete for vacancies even at modest concentrations to increase surface heterogeneity, as will be contextualized below using simulations. Spatial snapshots of the interfacial heterogeneity are provided in Figure S15, which show, in agreement with experiment, a more heterogeneous decane/aqueous interface. Water density profiles along the interface normal (to determine the Gibbs

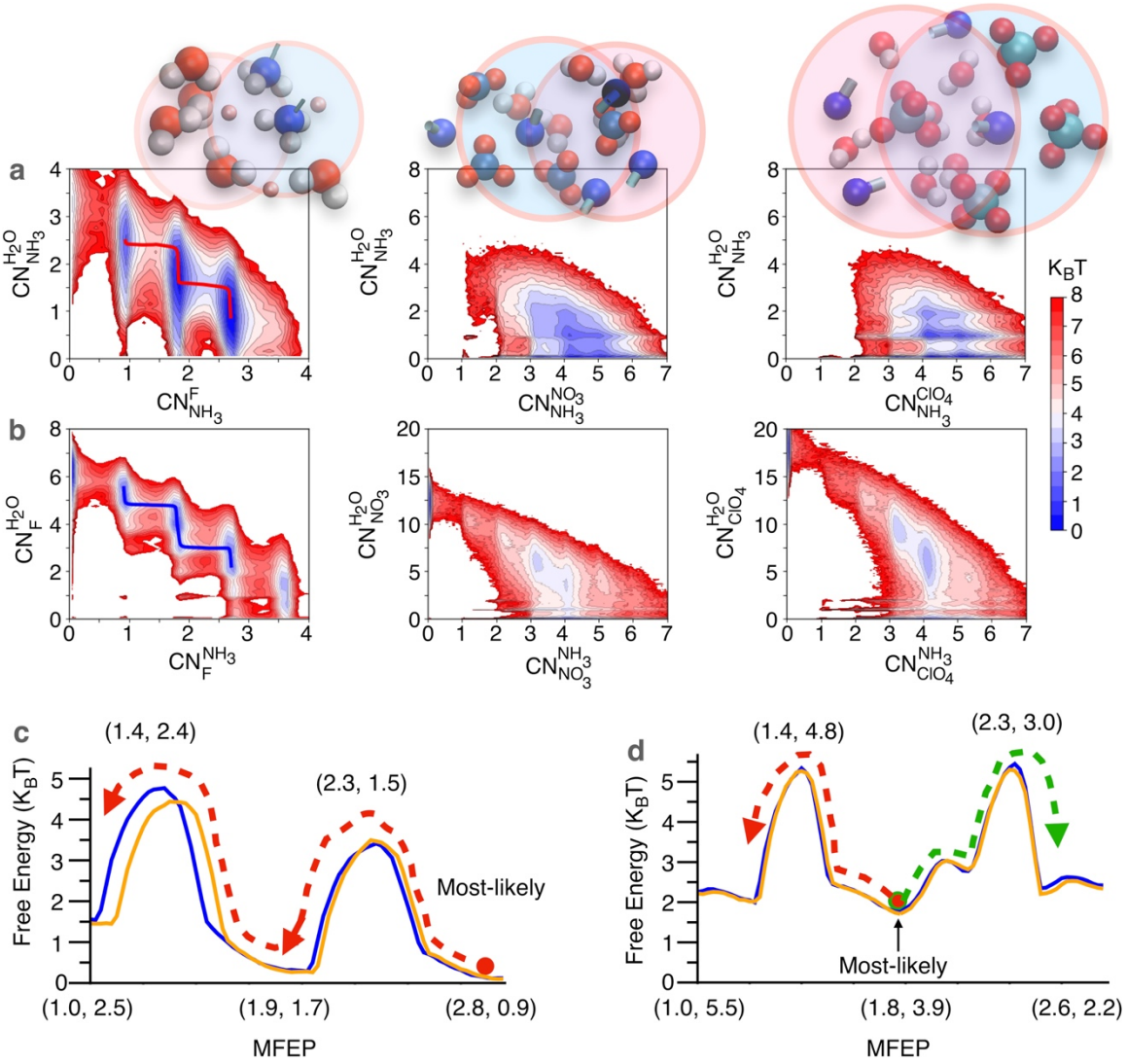

Figure 6. 2D free-energy surfaces showcasing how the anion coordination number of a ligand headgroup, CN^{A}_{NH3} where A = { F^-, NO_3^- and ClO_4^-} (a) and vice versa, CN^{NH3}_{A} (b) anti-correlate to the change in their water coordination numbers, CN^{H2O}_{NH3} and CN^{H2O}_{A} at the air/aqueous interface (see Figures S17 and S18 for the decane/water results). For F^-, there is a stepwise anticorrelation, while it is monotonous for the larger anions. The MFEPs are indicated by the red and blue solid lines in a and b for F^-. The free energy values along the MFEP for anion exchange around a ligand headgroup and vice versa are respectively presented in c and d for the air-water (blue trace) and oil -water (golden yellow trace) interfaces. The labels along the MFEP axis represent (CN^{A}_{NH3}, CN^{H2O}_{NH3}) and (CN^{NH3}_{A}, CN^{H2O}_{A}) in c and d, respectively.

Dividing Surface (GDS)) are given in Figure S16. The ion free energy profiles at the high concentration limit are given in Figure S17, which qualitatively match the adsorption equilibria measured by SFG. This agreement reinforces the MD simulations for elucidating ion, solvent, and ligand exchange mechanisms, which are averaged over in experiments. Finally, as will be discussed later for the air-water systems containing F^- ions at both high and low concentrations, we compare computed SFG spectral densities of the decoupled OH stretches in water (mimicking the case of isotope-diluted water) using the Skinner map[44-46] (see SI for details) to explain the water orientation and H-bonding or ion-water/ion-ion coordination at the interface, directly linking to the SFG experiments. It is worth mentioning that the surface morphology can be dynamic and influence the ligand-ion, ligand-solvent, and ion-solvent coordination near the interface. The free-energy landscapes describing these interactions, specifically the aforementioned exchange mechanisms, effectively (or on the average) account for potential surface morphological effects by averaging over

independent MD simulations (see supporting information).

To describe local coordination environments around the $-NH_3^+$ headgroups in the F^--rich (at a high concentration) systems, we plot free energy profiles vs. the distance between various species, W(r), in Figure 5. Specifically, the interaction strengths and structural organization between the headgroups, headgroups and waters, and headgroups and F^- ions are respectively elucidated in Figures 5a-c. From these profiles, one can readily identify free-energy minima describing metastable configurations of headgroups, water, and ions that persist over a surprisingly broad range of length scales, as indicated by shaded and numbered regimes. These scales correspond to concentric coordination spheres around a central N atom, depicted in Figure 5d. The grouping of chemical species into clusters is apparent from both the free energy surfaces and the iso-surface in Figure 5d. From Figure 5a, we find that decane/aqueous interfaces host smaller barriers for a ligand to exchange between local cluster states as compared to the air/aqueous interface. While the magnitude barrier reduction is modest, the differences point nonpolar phase-specific exchange dynamics of metastable clusters resulting in a more structurally heterogeneous decane/aqueous interface. In contrast, the W(r) profiles shown in Figures 5b and 5c, describe the $-NH_3^+$–water and $-NH_3^+$–F^- distance correlations, respectively, where the differences between the two interfaces are found to be negligible. Here, the hydration structures rapidly interconvert due to small barriers to yield spectroscopically similar observables at high ionic strength, in agreement with the SFG data in Figure 3a-3c. Interestingly, the barrier for removing an F^- anion from the 1st coordination shell of an ODA headgroup is ~5.25 k_BT, which is much larger than the barrier required for reorganizing interfacial water or ligands. This means that it is easier to exchange water or ODA molecules between assemblies than it is to remove a *surface inactive* F^- anion and that the interfacial microheterogeneity arises from ion pairing interactions that differ between the two interfaces, in agreement with experiment. Taken together, these results show that decane/aqueous interfaces are intrinsically more dynamic and chemically heterogeneous on a microscopic level, hosing a variety of instantaneous arrangements with variable compositions that that are enabled by competitive nonpolar phase solvation of ODA tails. This insight connects back to the small differences in binding free energies between the decane/aqueous and air/aqueous interface found in SFG measurements.

This microheterogeneity can be seen in the 2D free energy landscapes correlating $-NH_3^+$–F^- and $-NH_3^+$–water coordination numbers with headgroup–headgroup coordination numbers that plotted in Figure 5e. At the air/aqueous interface, we find that ~3 F^- ions are arranged about any given headgroup as to mediate interactions with the nearby ~2–4 other headgroups (Figures 5d and 5e) that comprise a nominal cluster. As the F^- coordination number reduces to 2 and then to 1 (Figure 5e), the number of nearby headgroups changes in a correlated stepwise fashion, mediated by charge screening and increased $-NH_3^+$–water coordination numbers. This general anti-correlation between coordination environments persists at the decane/aqueous interface; however, there are additional local minima highlighted in Figure 5e that demonstrate the existence of *isolated* ODA–F^- pairs and fully hydrated headgroups. These configurations exist due to the increased structural disorder and microscopic heterogeneity found at decane/aqueous interfaces that is absent at air/aqueous surfaces. We note here that our findings of functional assemblies and isolated amphiphiles at oil/aqueous interfaces underlies chemical and biological transport mechanisms via molecular, micellar or water finger-based means.[47-50] Simulations point to a mixture of solvation environments from metastable configurations that are enabled by tail solvation that encourages exchange by offsetting energetic penalties to dehydrating the headgroup. Furthermore, the fact that the $-NH_3^+$–water and $-NH_3^+$–F^- binding free energies (related to the barrier heights in Figure 5b and 5c) are identical at decane/aqueous and air/aqueous interfaces means that an enhanced entropic contribution to the free energies that arise from structural disorder driven by the tail-decane interactions are offset by an enthalpic contribution arising from clustering and solvation in the aqueous phase. It should be noted while the high charge-density hard F^- anions promote headgroup–headgroup interactions, the lower charge-density soft anions, NO_3^- and ClO_4^-, do not play the same role due to their weak association with the ODA headgroups (Section 7.2 in SI and Figure S18).

It is apparent that cluster metastability strongly correlates with the degree of water exposure. It is thus critical to determine the role of water in mediating the events of anion exchange around a headgroup as well as the events of ligand exchange around anions. In Figure 6a, we showcase distinct exchange mechanisms around a $-NH_3^+$ headgroup in the presence of F^-, NO_3^- or ClO_4^- at an air/aqueous interface. As mentioned previously, the most likely F^- coordination number with a given headgroup is ~3. In this configuration, water spontaneously exchanges until an activated high water coordination number is attained, after which one F^- ion can leave the first coordination shell, allowing the headgroup–F^-coordination environment to relax about the ~2 F^-

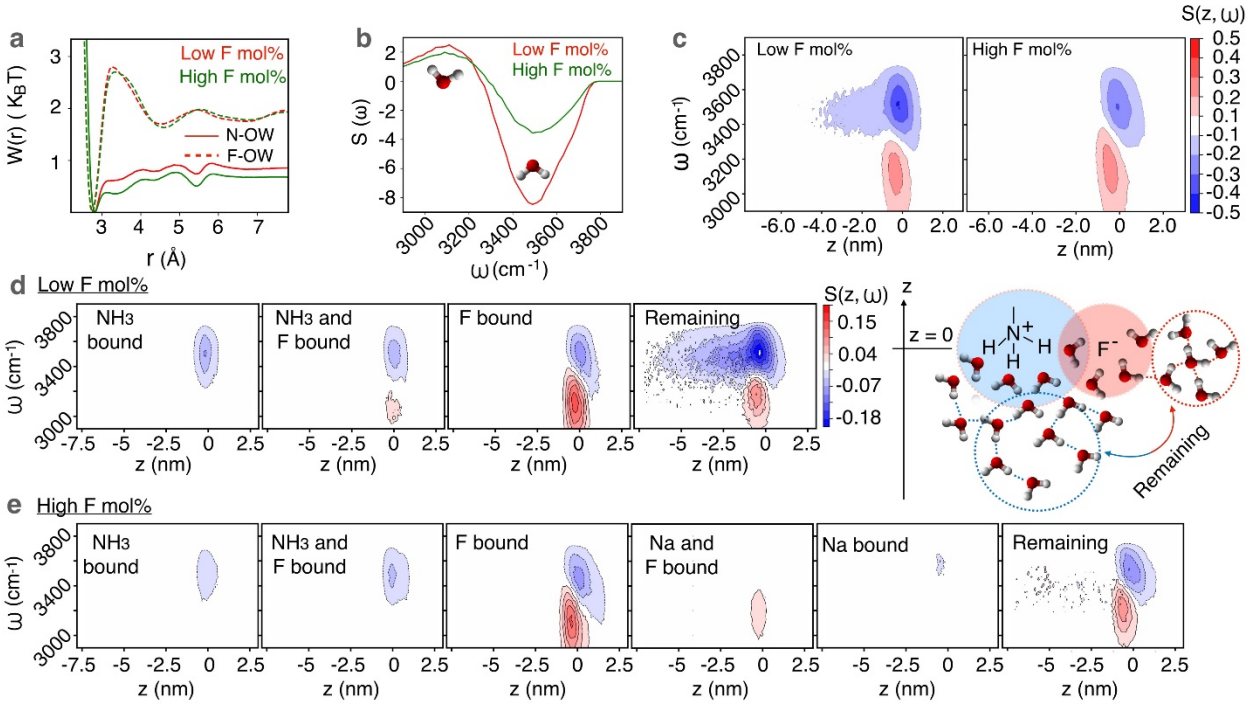

Figure 7. The effect of F^- concentration on the solvent structures and interaction strengths around the -NH_3^+ group and F^- ions at the air-water interface, reflected in the free-energy profiles of the N-OW and F-OW distances (a) and computed 1D spectra density (S(ω)) (b) and 2D spectral densities (S(z, ω)) (c) for the decoupled OH stretches (mimicking the OH stretch of HOD in D_2O). The 2D spectral densities are decomposed into the contributions from the groups of solvent waters bound to different charges groups/ions and the rest, shown for both low (d) and high (e) concentrations of F^- ions. The z = 0 represents the GDS and the cartoon illustrates the charged group/ion-specific solvation structures and alignments, leading to positive (OH pointing up) and negative signals (OH pointing down).

coordinate state. The same stepwise mechanism is followed in going to 1 F^-–coordinate state. From these surfaces, the stepwise minimum free–energy path (MFEP) computed using the String method[51] plotted in Figure 6c, reveals differences in the free energetics between the air/aqueous and decane/aqueous interfaces. Namely, in the first step of F^- dissociation, the activated water configuration faces the same barriers along the MFEP for air/aqueous and decane/aqueous interfaces. However, a shifted and slightly lower barrier to lose the second F^- anion along MFEP is found for the decane/aqueous. From the perspective of the F^- anion, the most–likely headgroup coordination number is ~2 (Figures 6c and 6d) whereby going to a state of increased F^- coordination or to a state with reduced F^- coordination are equally and symmetrically as probable. For NO_3^- and ClO_4^-, the stepwise mechanism of anion exchange or ligand exchange are not apparent; instead, a continuum of coordination states is observed, which is due to weaker anion association to ODA. For these anions, thermal energy–driven fluctuations in the coordination environment are enough to rapidly drive exchange events between coordination microstates, leading to a continua of coordination numbers.

To connect back to the experimental observations, particularly on the ionic concentration effects on the interfacial solvent interaction strengths and structures, we elaborate how the F^--water and -NH_3^+-water interaction strengths can orient water in terms of the computed SFG spectral densities for the OH stretches as given in Figure 7. The free energy profiles suggest that the F^- ions are always strongly solvated, showing minimal dependence on their concentrations, while the -NH_3^+ groups demonstrate enhanced solvation at the lower F^- concentration due to a reduced likelihood of interactions between -NH_3^+ and F^-. In Table S5, we present the populations of different F^- coordination numbers around -NH_3^+, indicating that at the low F^- concentration, the population of the state where 3 F^- ions coordinate with a single -NH_3^+ group significantly decreases, while the populations for 0, 1, and 2 F– coordination states increase. Notably, the number of F^--free -NH_3^+ groups doubles at the low F^- concentration. This shift has a dramatic impact on the orientation of interfacial water molecules, as evidenced by the spectral densities, S(ω) (Figure 7b). For the low F^- concentration, S(ω) has a more-than-

twice deep negative peak at ~3500 cm^{-1} when compared to the high F^- concentration. These peaks represent waters with OH pointing away (downwards) from the interface. The positive peak around 3100 cm^{-1}, representing waters with OH pointing towards (upwards) the interface, is also observed to be slightly higher for the low concentration. These trends are readily observed in SFG spectra given in Figure 3.

To provide a detailed picture of which specific water molecules along the interface normal give rise to these peaks, we present S(z, ω) in Figure 7c, which again is decomposed into the contributions from waters bound separately or jointly to the $-NH_3^+$ groups and the ions and the remaining waters (Figures 7d and 7e). For low F^- concentration, as anticipated, the only $-NH_3^+$-bound downward-oriented waters contribute to the negative peak. Waters trapped between $-NH_3^+$ and F^- ions contribute mostly to the negative peak and a little to the positive peak. The solely F^--bound waters contribute nearly equally to both the positive and negative peaks. This means an F^--bound water molecule has one OH pointing upward and strongly H-bonded to F^-, while its other OH points downward and is H-bonded to other water molecules. For the high F^- concentration, we find the same, along with contributions from waters trapped between Na^+ and F^- and solely Na^+-bound to the positive and negative peaks, respectively. The significant difference between the low and high concentration cases lies in the contribution from the remaining waters (not bound to ions or the ligand headgroups). In the case of the former, water molecules are oriented downwards deep into the bulk region (negative signal spreads down to >5 nm from the GDS), which is not the case for the latter. We attribute this to the aforementioned reduced ligand-ion coordination at the low F^- concentration that allows $-NH_3^+$ groups to polarize bulk water. It is also interesting to see that a sub-ensemble of waters that are not ion-bound can also be strongly H-bonded to each other and contribute to the low-frequency positive peak. We note here that while there is a *quantitative* difference between the experimental SFG and computed SFG spectral density, due to the neglect of couplings between the OH stretches in the latter, qualitatively both agree and complement each other in the findings of ionic concentration effects on the interfacial solvation structures and their spectroscopic characteristics.

The unexpected affinity of F^- for the surface is realized through ion pairing interactions and subsequent aggregation into metastable clusters that exchange ligand and water molecules vs. losing F^- ions that would otherwise destabilize clusters. The exchange and interactions between these metastable clusters rely on interactions with a nonpolar phase to break free, lowering the exchange barriers, resulting in scenarios where isolated headgroups or individual ion-pairs (and associated H-bonding networks) can be identified from the ensemble. This cluster 'escape route' does not exist at the air/aqueous interface, limiting the microheterogeneity of the interface and results in different time-averaged H-bonding spectra. In this regard, the discovery of a short–to–intermediate range ordering that is encoded by the surface microheterogeneity, a critical feature of liquids that form networks and functional aggregates in the context of balancing hydrophilic and hydrophobic interactions, provides a path forward in designing self-assembled interfaces with unique transport and chemical properties.

CONCLUSION

We show that competitive solvation of interfacial amphiphiles with a supposedly non-interacting nonpolar phase can lead to striking differences in equilibrium adsorption free energies and apparent H-bonding strengths. Classically, these would be understood in the framework of the Hofmeister series and Laws of Matching Water affinities; however, we show that a remarkable microheterogeneity emerges at oil/aqueous interfaces allows for a distribution of instantaneous local chemical environments and metastable clusters. Many of these transient environments are inaccessible to the amphiphiles without solvation in the neighboring non-polar phase. This insight feeds back into equilibrium and static pictures of the interface, where a homogeneous interface and H-bonding network is assumed; instead, we show that the solvating oil phase can facilitate the escape of isolated molecular species leading to surface roughness and molecular scale heterogeneity that plays a significant role in altering the rules for assembly and function, as evidenced by differences in the free energy of adsorption for hard, surface inactive anions. This insight into the balance and competition of hydrophilic and hydrophobic interactions is at the heart of phase separation in liquids, nanomaterials and bio-interfaces. This new insight obtained from surface specific spectroscopy and molecular dynamics simulations provides a path to shape and measure these instantaneous configurations to build local chemical environments capable of selective chemistry that is otherwise inaccessible to simple model systems.

EXPERIMENTAL SECTION

Reagents

NaSCN (99.99%), NaF (99.99%), NaCl (99.9%), NaBr (99.9%), $NaNO_3$ (99%), NaI (99.5%), and $NaClO_4$ (99.9%) were purchased from Sigma Aldrich. decane (99%) and chloroform (99%) was purchased from Thermo Fisher Scientific. Octadecylamine (ODA, 97%)

was purchased from Alfa–Aesar. Sodium hydroxide (NaOH) was purchased from Alfa–Aesar (98%) and hydrogen chloride (HCl) from Fisher Chemical (36.5 to 38.0%). All chemicals were used without further purification.

Solution preparation

ODA was dissolved in chloroform (1.5 mM) for air/aqueous experiments. ODA was dissolved in decane (1 mM) for decane/aqueous interface experiments. Stock solutions of metal salts (2 M for NaSCN, NaBr, $NaNO_3$, NaI, $NaClO_4$, 1 M for NaCl, 0.8 M for NaF) were prepared with ultrapure water from a Millipore water system and subsequently diluted to stated concentrations. The pH was adjusted with HCl (0.01 M, 0.1 M) and NaOH (0.01 M, 0.1 M) solutions.

Vibrational sum frequency generation spectroscopy (SFG)

For all interfaces, an aqueous phase containing different concentrations of electrolytes is contained in a Teflon dish. Air/aqueous interfaces are built by spreading 20 μL of ODA–chloroform solution (1.5 mM) on the top of aqueous solution. As the chloroform evaporates, a well–packed interfacial monolayer is formed and characterized by surface tension (Figure S1). Decane/aqueous interface are made by adding 40 μL of ODA–decane solution to the aqueous phase then allowing for the oil to spread out to homogeneously cover the surface. Based on previous ellipsometry measurements, the thickness of the oil phase is on the order of 100s of nm, thin enough to avoid substantial light attenuation.[12, 19] Vibrational sum frequency generation spectroscopy (SFG) using a custom–built system is detailed elsewhere.[21, 52-53] Briefly, broadband mid–infrared pulses (centered around 2050 cm^{-1} for SCN^- measurements, 2900 cm^{-1} for CH measurements, and 3400 cm^{-1} for H_2O measurements) and narrow–band near–infrared pulses (centered near 803 nm, with a 1 nm bandwidth at full width half maximum) are spatially and temporally overlapped at the sample interface at a 60° angle with respect to the upper surface normal. The radiated SFG signal is collected in a reflection geometry, polarization resolved, spectrally dispersed, and detected using a CCD camera (Newton, Andor). Static measurements are made after 30 minutes of equilibration. In all cases, the raw SFG intensity spectra are background subtracted and scaled to the nonresonant response of a gold film.

A Voigt profile describes the convolution of a Lorentzian and a Gaussian line shape and is used to fit the SFG signal from SCN^- chromophores:[54]

$$I_{\mathrm{SFG}} \propto \left| \chi_{\mathrm{NR}}^{(2)} e^{i\Phi} + \sum A_q \frac{w\left(\frac{\omega_q - \omega_{IR} + i\Gamma_{L,q}}{\sqrt{2}\Gamma_{G,q}}\right)}{\sqrt{2\pi}\Gamma_{G,q}} \right|^2 \qquad \text{(Eq. 1)}$$

where $\chi_{NR}^{(2)}$ is the nonresonant response, ω_{IR} is the frequency of the incident IR light, ω_q and A_q are the resonant transition frequency and amplitude, respectively. $\Gamma_{L,q}$ and $\Gamma_{G,q}$ are the linewidth of the q^{th}–mode for Lorentzian and Gaussian components, respectively. To simplify fitting, we set Lorentzian and Gaussian linewidths to be equal. $w(z)$ is a Faddeeva function.[55] The phase angle, φ,[56] mixes in contributions from polarized bulk water via the $\chi^{(3)}$–effect[14, 53] that is included in $\chi_{NR}^{(2)}$.[41, 53] SFG spectra are fit to Eq. 1 to extract parameters describing the surface population of SCN^- as discussed in the text. As for the SFG spectra in the CH region, a coherent sum of Lorentzians is fit resonant peaks to extract the structure of ODA at the interfaces.[16, 52] Relevant fitting parameters are summarized in Table S3 and S4. Details of the spectral processing used to correct OH spectra are provided in the SI.

ASSOCIATED CONTENT

A supporting information document is provided that contains surface tension measurements, supporting SFG experiments and analyses, infrared spectra, and simulation details with additional analyses.

AUTHOR INFORMATION

Corresponding Author

*** pans@ameslab.gov**

*** carrillojy@ornl.gov**

*** roys@ornl.gov**

*** doughtybl@ornl.gov**

Author Contributions

All authors participated in manuscript preparation and have given approval to the final version of the manuscript. There are no conflicts to declare.

Funding Sources

Work by P.S., U.I.P., S.R., and B.D. was supported by the US Department of Energy, Office of Science, Basic Energy Sciences, Chemical Sciences, Geosciences, and Biosciences Division, Separation Sciences. J.-M.Y.C.

performed MD simulations partially conducted at the Center for Nanophase Materials Sciences, which is a DOE Office of Science User Facility. R.L.S. was supported by the Center for Closing the Carbon Cycle, an Energy Frontier Research Center funded by the U.S. Department of Energy (DOE), Office of Science, Basic Energy Sciences (BES), under Award Number DE-SC0023427. This work was produced by UT–Battelle LLC under Contract No. AC05–00OR22725 with the U. S. Department of Energy.

REFERENCES

1. Das, S.; Lin, Y.-H.; Vernon, R. M.; Forman-Kay, J. D.; Chan, H. S., Comparative roles of charge, π , and hydrophobic interactions in sequence-dependent phase separation of intrinsically disordered proteins. *Proceedings of the National Academy of Sciences* **2020,** *117* (46), 28795-28805.
2. The many phases of biomolecular condensates. *Nature Chemistry* **2024,** *16* (7), 1035-1036.
3. Watson, J. L.; Seinkmane, E.; Styles, C. T.; Mihut, A.; Krüger, L. K.; McNally, K. E.; Planelles-Herrero, V. J.; Dudek, M.; McCall, P. M.; Barbiero, S.; Vanden Oever, M.; Peak-Chew, S. Y.; Porebski, B. T.; Zeng, A.; Rzechorzek, N. M.; Wong, D. C. S.; Beale, A. D.; Stangherlin, A.; Riggi, M.; Iwasa, J.; Morf, J.; Miliotis, C.; Guna, A.; Inglis, A. J.; Brugués, J.; Voorhees, R. M.; Chambers, J. E.; Meng, Q.-J.; O'Neill, J. S.; Edgar, R. S.; Derivery, E., Macromolecular condensation buffers intracellular water potential. *Nature* **2023,** *623* (7988), 842-852.
4. Welles, R. M.; Sojitra, K. A.; Garabedian, M. V.; Xia, B.; Wang, W.; Guan, M.; Regy, R. M.; Gallagher, E. R.; Hammer, D. A.; Mittal, J.; Good, M. C., Determinants that enable disordered protein assembly into discrete condensed phases. *Nature Chemistry* **2024,** *16* (7), 1062-1072.
5. Denesyuk, N. A.; Thirumalai, D., How do metal ions direct ribozyme folding? *Nature Chemistry* **2015,** *7* (10), 793-801.
6. Arnold, F. H.; Haymore, B. L., Engineered Metal-Binding Proteins: Purification to Protein Folding. *Science* **1991,** *252* (5014), 1796-1797.
7. O'Connell-Danes, J. G.; Ngwenya, B. T.; Morrison, C. A.; Love, J. B., Selective separation of light rare-earth elements by supramolecular encapsulation and precipitation. *Nature Communications* **2022,** *13* (1), No.4497.
8. Shao, B.; Fu, H.; Aprahamian, I., A molecular anion pump. *Science* **2024,** *385* (6708), 544-549.
9. Chen, H.; Fraser Stoddart, J., From molecular to supramolecular electronics. *Nature Reviews Materials* **2021,** *6* (9), 804-828.
10. Adkins, R.; Kolvin, I.; You, Z.; Witthaus, S.; Marchetti, M. C.; Dogic, Z., Dynamics of active liquid interfaces. *Science* **2022,** *377* (6607), 768-772.
11. Luo, G.; Malkova, S.; Yoon, J.; Schultz, D. G.; Lin, B.; Meron, M.; Benjamin, I.; Vanýsek, P.; Schlossman, M. L., Ion Distributions near a Liquid-Liquid Interface. *Science* **2006,** *311* (5758), 216-218.
12. Lin, L.; Liu, Z.; Premadasa, U. I.; Li, T.; Ma, Y.-Z.; Sacci, R. L.; Katsaras, J.; Hong, K.; Collier, C. P.; Carrillo, J.-M. Y.; Doughty, B., The Unexpected Role of Cations in the Self-Assembly of Positively Charged Amphiphiles at Liquid/Liquid Interfaces. *The Journal of Physical Chemistry Letters* **2022,** *13* (46), 10889-10896.
13. Litman, Y.; Chiang, K.-Y.; Seki, T.; Nagata, Y.; Bonn, M., Surface stratification determines the interfacial water structure of simple electrolyte solutions. *Nature Chemistry* **2024,** *16* (4), 644-650.
14. Eisenthal, K. B., Liquid Interfaces Probed by Second-Harmonic and Sum-Frequency Spectroscopy. *Chem Rev* **1996,** *96* (4), 1343-1360.
15. Chang, T.-M.; Dang, L. X., Recent Advances in Molecular Simulations of Ion Solvation at Liquid Interfaces. *Chem Rev* **2005,** *106* (4), 1305-1322.
16. Chen, X.; Yang, T.; Kataoka, S.; Cremer, P. S., Specific Ion Effects on Interfacial Water Structure near Macromolecules. *Journal of the American Chemical Society* **2007,** *129* (40), 12272-12279.
17. Petersen, P. B.; Saykally, R. J., On the Nature of Ions at the Liquid Water Surface. *Annual Review of Physical Chemistry* **2006,** *57* (1), 333-364.
18. Seki, T.; Yu, C.-C.; Chiang, K.-Y.; Greco, A.; Yu, X.; Matsumura, F.; Bonn, M.; Nagata, Y., Ions Speciation at the Water–Air Interface. *Journal of the American Chemical Society* **2023,** *145* (19), 10622-10630.
19. Premadasa, U. I.; Ma, Y.-Z.; Sacci, R. L.; Bocharova, V.; Thiele, N. A.; Doughty, B., Understanding Self-Assembly and the Stabilization of Liquid/Liquid Interfaces: The Importance of Ligand Tail Branching and Oil-Phase Solvation. *Journal of Colloid and Interface Science* **2022,** *609*, 807-814.
20. Chen, Y.; Jena, K. C.; Roke, S., From Hydrophobic to Hydrophilic: The Structure and Density of the Hexadecane Droplet/Alkanol/Water Interface. *The Journal of Physical Chemistry C* **2015,** *119* (31), 17725-17734.
21. Chowdhury, A. U.; Taylor, G. J.; Bocharova, V.; Sacci, R. L.; Luo, Y.; McClintic, W. T.; Ma, Y.-Z.; Sarles, S. A.; Hong, K.; Collier, C. P.; Doughty, B., Insight into the Mechanisms Driving the Self-Assembly of Functional Interfaces: Moving from Lipids to Charged Amphiphilic Oligomers. *Journal of the American Chemical Society* **2019,** *142* (1), 290-299.
22. Nave, S.; Mandin, C.; Martinet, L.; Berthon, L.; Testard, F.; Madic, C.; Zemb, T., Supramolecular organisation of tri-n-butyl phosphate in organic diluent on approaching third phase transition. *Physical Chemistry Chemical Physics* **2004,** *6* (4), 799-808.
23. Mu, J.; Motokawa, R.; Akutsu, K.; Nishitsuji, S.; Masters, A. J., A Novel Microemulsion Phase

Transition: Toward the Elucidation of Third-Phase Formation in Spent Nuclear Fuel Reprocessing. *The Journal of Physical Chemistry B* **2018,** *122* (4), 1439-1452.
24. Piradashvili, K.; Alexandrino, E. M.; Wurm, F. R.; Landfester, K., Reactions and Polymerizations at the Liquid–Liquid Interface. *Chem Rev* **2015,** *116* (4), 2141-2169.
25. Qiao, B.; Ferru, G.; Olvera de la Cruz, M.; Ellis, R. J., Molecular Origins of Mesoscale Ordering in a Metalloamphiphile Phase. *ACS Central Science* **2015,** *1* (9), 493-503.
26. Shelby, S. A.; Castello-Serrano, I.; Wisser, K. C.; Levental, I.; Veatch, S. L., Membrane phase separation drives responsive assembly of receptor signaling domains. *Nature Chemical Biology* **2023,** *19* (6), 750-758.
27. Otten, D. E.; Shaffer, P. R.; Geissler, P. L.; Saykally, R. J., Elucidating the mechanism of selective ion adsorption to the liquid water surface. *Proceedings of the National Academy of Sciences* **2012,** *109* (3), 701-705.
28. Li, Q.; Xie, S.; Liang, Z.; Meng, X.; Liu, S.; Girault, H. H.; Shao, Y., Fast Ion-Transfer Processes at Nanoscopic Liquid/Liquid Interfaces. *Angewandte Chemie International Edition* **2009,** *48* (43), 8010-8013.
29. Borsley, S.; Leigh, D. A.; Roberts, B. M. W., Molecular Ratchets and Kinetic Asymmetry: Giving Chemistry Direction. *Angewandte Chemie International Edition* **2024,** *63* (23), e202400495.
30. Gurau, M. C.; Lim, S.-M.; Castellana, E. T.; Albertorio, F.; Kataoka, S.; Cremer, P. S., On the Mechanism of the Hofmeister Effect. *Journal of the American Chemical Society* **2004,** *126* (34), 10522-10523.
31. Jungwirth, P.; Cremer, P. S., Beyond Hofmeister. *Nature Chemistry* **2014,** *6* (4), 261-263.
32. Collins, K. D., Charge density-dependent strength of hydration and biological structure. *Biophysical Journal* **1997,** *72* (1), 65-76.
33. Collins, K. D., The behavior of ions in water is controlled by their water affinity. *Quarterly Reviews of Biophysics* **2019,** *52*, 1–19.
34. Stiopkin, I. V.; Jayathilake, H. D.; Bordenyuk, A. N.; Benderskii, A. V., Heterodyne-Detected Vibrational Sum Frequency Generation Spectroscopy. *Journal of the American Chemical Society* **2008,** *130* (7), 2271-2275.
35. Tian, C.-S.; Shen, Y. R., Isotopic Dilution Study of the Water/Vapor Interface by Phase-Sensitive Sum-Frequency Vibrational Spectroscopy. *Journal of the American Chemical Society* **2009,** *131* (8), 2790-2791.
36. de Beer, A. G. F.; Samson, J.-S.; Hua, W.; Huang, Z.; Chen, X.; Allen, H. C.; Roke, S., Direct comparison of phase-sensitive vibrational sum frequency generation with maximum entropy method: Case study of water. *The Journal of Chemical Physics* **2011,** *135* (22), 224701.
37. Backus, E. H. G.; Garcia-Araez, N.; Bonn, M.; Bakker, H. J., On the Role of Fresnel Factors in Sum-Frequency Generation Spectroscopy of Metal–Water and Metal-Oxide–Water Interfaces. *The Journal of Physical Chemistry C* **2012,** *116* (44), 23351-23361.
38. Wen, Y.-C.; Zha, S.; Liu, X.; Yang, S.; Guo, P.; Shi, G.; Fang, H.; Shen, Y. R.; Tian, C., Unveiling Microscopic Structures of Charged Water Interfaces by Surface-Specific Vibrational Spectroscopy. *Physical Review Letters* **2016,** *116* (1), 016101.
39. Pullanchery, S.; Kulik, S.; Rehl, B.; Hassanali, A.; Roke, S., Charge transfer across C–H···O hydrogen bonds stabilizes oil droplets in water. *Science* **2021,** *374* (6573), 1366-1370.
40. Gera, R.; Bakker, H. J.; Franklin-Mergarejo, R.; Morzan, U. N.; Falciani, G.; Bergamasco, L.; Versluis, J.; Sen, I.; Dante, S.; Chiavazzo, E.; Hassanali, A. A., Emergence of Electric Fields at the Water–C12E6 Surfactant Interface. *Journal of the American Chemical Society* **2021,** *143* (37), 15103-15112.
41. Ohno, P. E.; Wang, H.-f.; Geiger, F. M., Second-order spectral lineshapes from charged interfaces. *Nature Communications* **2017,** *8* (1), No.1032.
42. Smolentsev, N.; Smit, W. J.; Bakker, H. J.; Roke, S., The interfacial structure of water droplets in a hydrophobic liquid. *Nature Communications* **2017,** *8* (1), No.15548.
43. Rehl, B.; Ma, E.; Parshotam, S.; DeWalt-Kerian, E. L.; Liu, T.; Geiger, F. M.; Gibbs, J. M., Water Structure in the Electrical Double Layer and the Contributions to the Total Interfacial Potential at Different Surface Charge Densities. *Journal of the American Chemical Society* **2022,** *144* (36), 16338-16349.
44. Lin, Y. S.; Auer, B. M.; Skinner, J. L., Water structure, dynamics, and vibrational spectroscopy in sodium bromide solutions. *The Journal of Chemical Physics* **2009,** *131* (14), 144511.
45. Gruenbaum, S. M.; Pieniazek, P. A.; Skinner, J. L., Vibrational spectroscopy of water in hydrated lipid multi-bilayers. II. Two-dimensional infrared and peak shift observables within different theoretical approximations. *The Journal of Chemical Physics* **2011,** *135* (16), 164506
46. Roy, S.; Gruenbaum, S. M.; Skinner, J. L., Theoretical vibrational sum-frequency generation spectroscopy of water near lipid and surfactant monolayer interfaces. *The Journal of Chemical Physics* **2014,** *141* (18), 18C502.
47. Clark, A. E., Amphiphile-Based Complex Fluids: The Self-Assembly Ensemble as Protagonist. *ACS Central Science* **2018,** *5* (1), 10-12.
48. Qiao, B.; Muntean, J. V.; Olvera de la Cruz, M.; Ellis, R. J., Ion Transport Mechanisms in Liquid–Liquid Interface. *Langmuir* **2017,** *33* (24), 6135-6142.
49. Devlin, S. W.; Benjamin, I.; Saykally, R. J., On the mechanisms of ion adsorption to aqueous

interfaces: air-water vs. oil-water. *Proceedings of the National Academy of Sciences* **2022,** *119* (42), e2210857119.
50. Liang, Z.; Bu, W.; Schweighofer, K. J.; Walwark, D. J.; Harvey, J. S.; Hanlon, G. R.; Amoanu, D.; Erol, C.; Benjamin, I.; Schlossman, M. L., Nanoscale view of assisted ion transport across the liquid–liquid interface. *Proceedings of the National Academy of Sciences* **2018,** *116* (37), 18227-18232.
51. E, W.; Ren, W.; Vanden-Eijnden, E., Simplified and improved string method for computing the minimum energy paths in barrier-crossing events. *The Journal of Chemical Physics* **2007,** *126* (16), 164103.
52. Lin, L.; Chowdhury, A. U.; Ma, Y.-Z.; Sacci, R. L.; Katsaras, J.; Hong, K.; Collier, C. P.; Carrillo, J.-M. Y.; Doughty, B., Ion Pairing Mediates Molecular Organization Across Liquid/Liquid Interfaces. *ACS Applied Materials & Interfaces* **2021,** *13* (28), 33734-33743.
53. Premadasa, U. I.; Bocharova, V.; Lin, L.; Genix, A.-C.; Heller, W. T.; Sacci, R. L.; Ma, Y.-Z.; Thiele, N. A.; Doughty, B., Tracking Molecular Transport Across Oil/Aqueous Interfaces: Insight into "Antagonistic" Binding in Solvent Extraction. *The Journal of Physical Chemistry B* **2023,** *127* (21), 4886-4895.
54. Chen, S.-L.; Fu, L.; Gan, W.; Wang, H.-F., Homogeneous and inhomogeneous broadenings and the Voigt line shapes in the phase-resolved and intensity sum-frequency generation vibrational spectroscopy. *The Journal of Chemical Physics* **2016,** *144* (3), 034704.
55. Hore, D. K., Phase of the second-order susceptibility in vibrational sum frequency generation spectroscopy: Origins, utility, and measurement techniques. *The Journal of Chemical Physics* **2024,** *161* (6), 060902.
56. Ohno, P. E.; Saslow, S. A.; Wang, H.-f.; Geiger, F. M.; Eisenthal, K. B., Phase-referenced nonlinear spectroscopy of the α-quartz/water interface. *Nature Communications* **2016,** *7* (1), No.13587.

Graphical abstract